Superatom Pruning by Diphosphine Ligands as a Chemical Scissor

Yu-Ming Tseng, Jian-Hong Liao, Tzu-Hao Chiu, Hao Liang, Samia Kahlal, Jean-Yves Saillard, C W Liu

Superatom Pruning by Diphosphine Ligands as a Chemical Scissor

Yu-Ming Tseng,[a] Jian-Hong Liao,[a] Tzu-Hao Chiu,[a] Hao Liang,[b] Samia Kahlal,[b] Jean-Yves Saillard,[b,] C. W. Liu [a,]**

[a] Department of Chemistry, National Dong Hwa University, Hualien 97401, Taiwan (Republic of China).

[b] Univ Rennes, CNRS, ISCR-UMR 6226, F-35000 Rennes, France

ABSTRACT

A two-electron silver superatom, $[Ag_6\{S_2P(O^iPr)_2\}_4(dppm)_2]$ (**1**), was synthesized by adding dppm (bis(diphenylphosphino)methane) into $[Ag_{20}\{S_2P(O^iPr)_2\}_{12}]$ (8e). It was characterized by single-crystal crystallography, multinuclear NMR spectroscopy, ESI-MS, DFT and TD-DFT calculations. The added dppm ligands, which carry out the nanocluster-to-nanocluster transformation, act as a chemical scissor to prune the nanocluster geometrically from an icosahedron-based Ag_{20} NC to an octahedral Ag_6 NC and electronically from eight-electron to two-electron. Eventually dppm was involved in the protective shell to form a new heteroleptic NC. The temperature-dependent NMR spectroscopy confirms its fluxional behavior, showing the fast atomic movement at ambient temperature. Compound **1** exhibits a bright yellow emission under

UV irradiation at ambient temperature with a quantum yield of 16.3%. This work demonstrates a new methodology to achieve nanocluster-to-nanocluster transformation via step-wise synthesis.

INTRODUCTION

The chemistry of ligand-protected atom-precise metal nanoclusters (NCs) is currently flourishing, boosted by the intense interest in their unique properties that are substantially different from their corresponding bulk materials, with various fields of potential applications.[1-3] In this context, altering the composition, shape, and electronic configuration of NCs at the atomic level will sensitively induce significant changes for fine-tuning optical properties.[4] Strategies such as galvanic replacement,[5-6] ligand exchange,[7-8] and thermally-induced structural change[9-10] are commonly used to control cluster-to-cluster transformations. Such atomic-level molecular surgery on a specific site is currently an extremely challenging project,[11] and developing new methodologies in molecular engineering is an urgent need. Our previous report on atomically precise Ag_{20} NCs revealed a centered icosahedron as $[Ag_{13}]^{5+}$ kernel surrounded by seven Ag atoms and twelve dithiophosphate (dtp) ligands.[12] It has been further confirmed that the electronic property of those homoleptic $M_{20}L_{12}$ (L = dtp or dsep; dsep = diselenophosphate) NCs can be tuned by doping heterometal such as Pd, Pt, Cu, and Au.[8,13-17] However, these NCs maintain the same nuclearity and number of ligands. Thus, it is expected that reacting our easy-to-synthesize and neutral Ag_{20} NCs with heteroligands would affect their structure and properties. In this work, we report a facile way to reach NC pruning from an 8-electron heptacapped centered icosahedral Ag_{20} NC to a 2-electron octahedral Ag_6 NC. It is noteworthy that most of the known Ag_6 octahedral clusters are composed of solely Ag(I), *i.e.* are 0-electron species.[18-19] Although 2-electron $[Ag_6]^{4+}$

cores have also been reported, they constitute kernels embedded in larger metal cages.[20-24] To our knowledge, there is only one exception of a 2-electron octahedral hexanuclear silver species that was recently reported by Liu *et al.*, which is protected by trithiane and alkynyl ligands.[25] In any case, reports on small superatomic silver clusters remain scarce.[9] The synthesis, characterization, and structural analysis of a new heteroleptic 2-electron Ag_6 NC is discussed below.

RESULTS AND DISCUSSION

The reaction was carried out by adding 13 equiv. of dppm (dppm = 1, 1-bis(diphenylphosphino)methane) to $[Ag_{20}\{S_2P(O^iPr)_2\}_{12}]$ (abbrev. as Ag_{20}) in THF, and the reaction was kept stirring in the dark at 40 °C overnight. The reaction was terminated when the solution color changed from dark reddish brown to yellowish brown. The resulting product was further purified with methanol to yield $[Ag_6\{S_2P(O^iPr)_2\}_4(dppm)_2]$ (**1**) as a yellow precipitate. It is of note that a large excess of dppm is necessary for obtaining **1** in good yield, indicating that the extra dppm ligands act to cut the Ag_{20} NC into fragments. Thus, the destabilization under mild conditions of $[Ag_{20}\{S_2P(O^iPr)_2\}_{12}]$ in the presence of dppm ligands leads to cluster pruning from a capped icosahedral structure to an octahedron. Interestingly, the superatomic electron count is also modified from 8 ($1S^2\ 1P^6$ configuration) in Ag_{20} to 2 ($1S^2$ configuration) in **1**, maintaining a closed-shell configuration from $[Ag_{13}]^{5+}$ to $[Ag_6]^{4+}$ (*vide infra*.). The dppm ligand not only plays the role of a chemical scissor but also eventually participates in the protective layer. Generally, heteroleptic Ag NCs co-protected by diphosphines are prepared through a one-pot process or mixing all the precursors in a specific sequence.[26-28] Thus, the synthesis reported herein is a two-step process: (i) preparation of an 8-e Ag NC; (ii) adding dppm ligands under mild reaction conditions (Scheme 1), the driving force of the reaction originating from the dppm excess.

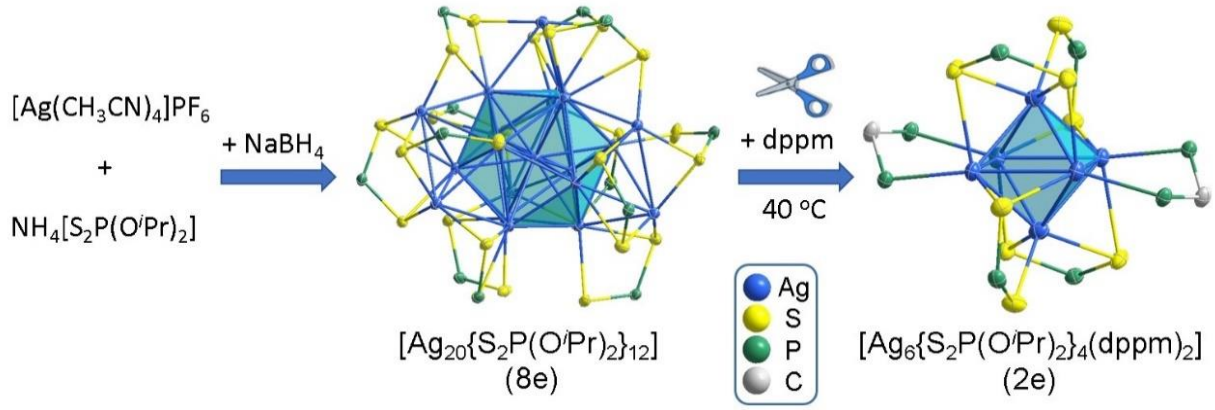

Scheme 1. Schematic representation of a two-step process in the synthesis of **1**.

Compound **1** crystallizes in the $P\bar{1}$ space group, with two half-molecules in the asymmetric unit. Thus, the crystal structure contains two symmetry-independent molecules (**I** and **II**), each one being of C_i symmetry (Figure 1). Both comprises an Ag_6 octahedron, two dppm ligands bridging opposite edges, and four dtp ligands bridging four among the eight triangular faces of the Ag_6 octahedron. The two molecules differ slightly in the connectivity of their dtp ligands. In each molecule, the four dithiophosphates can be separated into two L_A and two L_B ligands with respect to their coordination patterns. In molecule I (Figure 1a), L_A exhibit a trimetallic tetraconnectivity (η^3: μ_2, μ_2) and L_B a trimetallic triconnectivity (η^3: μ_1, μ_2). In molecule II (Figure 1b), L_A is shifted to one side, leading to the non-bonding S5…Ag4 separation (3.728(2) Å), which can be compared with the corresponding S2-Ag3 bonding distance (2.841(2) Å) in molecule **I**. Thus, the coordination mode of L_A shifts from trimetallic tetraconnectivity in **I** to bimetallic triconnectivity (η^3: μ_1, μ_2) in **II**. There are indications that in **I** the position of S1 of L_A is in close non-bonding contact (2.935 Å) with one adjacent proton on the phenyl group (Figure 1c). By comparison, in **II**, the S6 counterpart has more intramolecular contacts with three adjacent protons in the 2.957-2.979 Å range (Figure 1d), which could be one of the reasons to account for the L_A shift in **II**. In addition,

both molecules **I** and **II** show similar intermolecular S…H interactions (2.925 Å in **I** and 2.806 Å in **II**) along the crystallographic *b* axis (Figure S1). However, such weak interactions are easily destroyed in solution, due to the NMR-evidenced easy molecular mobility (*vide infra*). It is worth noting that the Ag…Ag distances (avg. 2.8490(9) Å and avg. 2.8239(10) Å in **I** and **II**, respectively) are comparable to that in the related octahedral 2-electron NC $[Ag_6(3S)_4(OTf)_4]$ (3S = 1,3,5-trithiane, OTf = trifluoromethanesulfonate),[25] (avg. 2.8006 Å). On the other hand, they are significantly shorter than that in the 0-electron silver(I) octahedral clusters such as $Ag_6(bmt)_6$ (avg. 3.1939 Å, bmt = 2-benzimidazolethiolate),[18] $[Ag_6(dppm)_2(C{\equiv}CFc)_4(CH_3OH)_2]^{2+}$ (avg. 3.028 Å),[19] and $[Ag_6(3S)_4(C{\equiv}C^tBu)_4]^{2+}$ (avg. 2.9000 Å).[19]. Selected bond lengths and angles are summarized in Table 1.

Table 1. Selected bond distances (Å) and angles (deg.) of **1**.

	X-ray		DFT
	Molecule I	Molecule II	
Ag…Ag	2.7530(9) – 3.0478(9), avg. 2.8490(9)	2.7665(10) – 2.8783(9), avg. 2.8239(10)	2.810-3.000 avg. 2.880
S-Ag	2.519(2) – 2.968(2), avg. 2.739(2)	2.581(2) – 2.945(2), avg. 2.706(2)	2.547-2.907 avg 2.747
P-Ag	2.4679(19) – 2.5077(19), avg. 2.4878(19)	2.474(2) – 2.499(2), avg. 2.487(2)	2.486-2.517 avg. 2.501
P…P bite	3.112(3)	3.094(3)	3.109

S…S bite	3.382(3) – 3.445(3), avg. 3.414(3)	3.350(4) – 3.437(3), avg. 3.394(4)	3.388-3.468 avg. 3.428
∠P-C-P	116.1(4)	113.7(4)	115
∠S-P-S	116.75(13) - 120.06(13), avg. 118.41(13)	115.52(14) - 119.13(14), avg. 117.33(14)	116-121 avg. 119

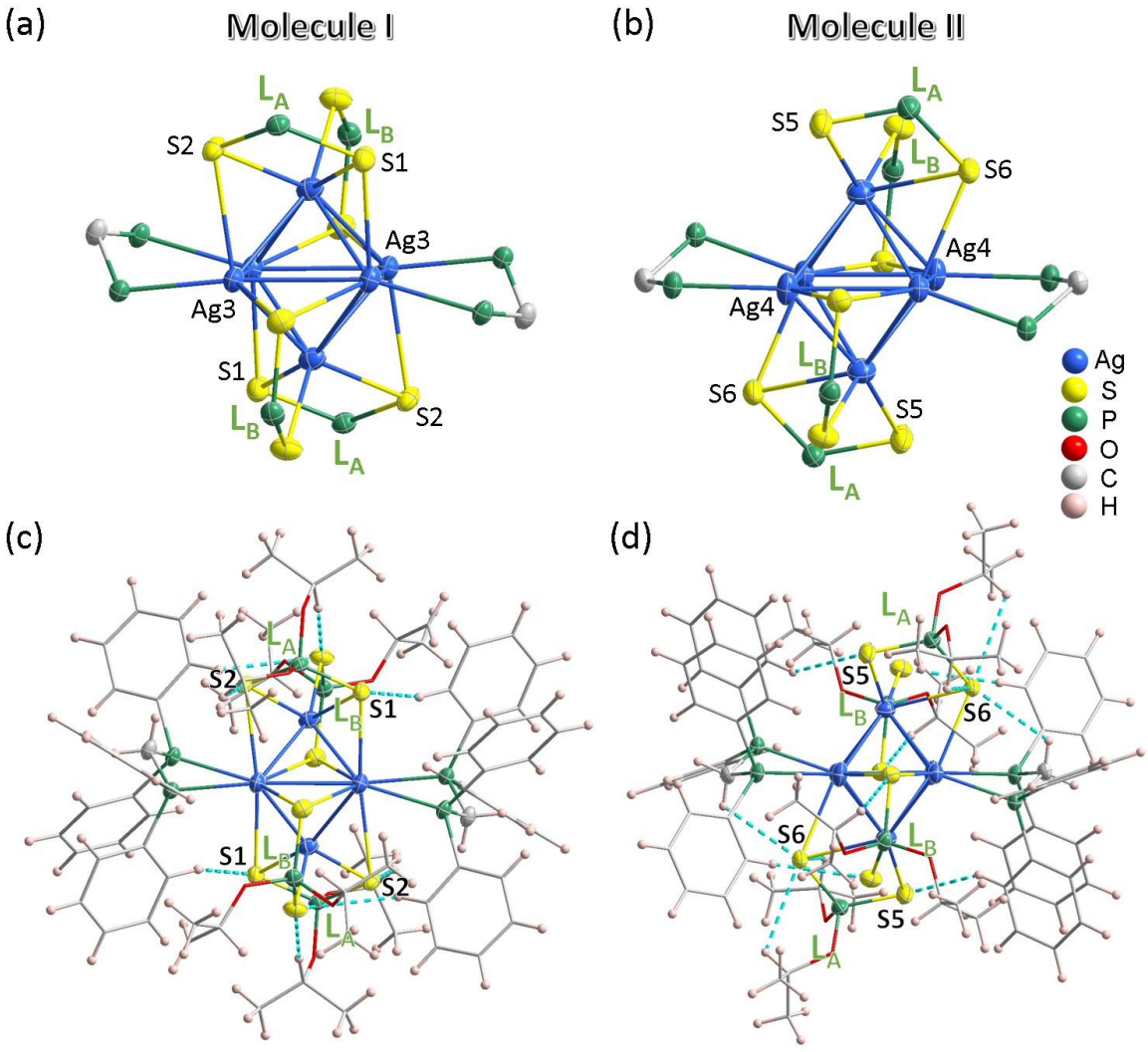

Figure 1. (a) The ORTEP drawing (30% probability) of molecule I and (b) molecule II in $[Ag_6\{S_2P(O^iPr)_2\}_4(dppm)_2]$, isopropoxy and phenyl groups were omitted for clarity. (c) The intramolecular S…H interactions in molecule I and (d) molecule II in the total structure of **1**.

The VT $^{31}P\{^1H\}$ NMR spectrum (Figure 2a) shows a single resonance of the dtp ligands at 103.2 ppm and a septet peak at 0.61 ppm for the dppm ligands at ambient temperature, then broadened at 223K, and eventually displaying clearer splitting patterns at 183K. In the $^{31}P\{^1H\}$ NMR spectrum at 183K, two resonances at 102.1 and 105.0 ppm with an equal integration ratio correspond to the two distinct L_A and L_B coordination modes of dtp ligands. A doublet peak at 0.36 ppm with an average coupling constant of 325 Hz indicates the direct coupling between ^{31}P of dppm and $^{107}Ag/^{109}Ag$ nuclei (Figure 2b). This resonance becomes a broad peak at 233K and splits into a doublet at 213 K. However, scalar couplings of $^1J(^{31}P\text{-}^{107}Ag)$ and $^1J(^{31}P\text{-}^{109}Ag)$ remain un-resolved upon decreasing the temperature to 183K. It can be attributed to the fluxional nature of **1**. As a result, a broad doublet (FWHM = 115 Hz) is observed at 183K instead of a pseudo doublet of doublets for a heteronuclear AX spin system. The splitting pattern is correlated to each dppm phosphorus atom connecting to one silver (Figure 2d). The low-temperature spectra are well-matching with the solid-state structure. Interestingly, a septet pattern observed at 0.61 ppm with an average coupling constant ($^1J(^{31}P\text{-}^{107,109}Ag)$ of 72 Hz (Figure 2c) suggests that each phosphorus nucleus is coupled with six magnetically equivalent silver nuclei. The phenomenon can be attributed to a fast molecular motion at room temperature. The molecular mobility can also be observed in the VT ^1H spectrum (Figure S6). The chemical shift of the dtp methine protons is at 4.48 ppm at room temperature and splits at 183K into two sets at 3.66 and 4.85 ppm with equal intensity, corresponding to the two L_A and L_B coordination environments. Both temperature-

dependent NMR spectra confirm its fluxional behavior, which is directly visible, especially through the close proximity between P(dppm) and Ag. In contrast, a two-bond coupling between P(dtp) and Ag is not observed in the $^{31}P\{^{1}H\}$ spectrum and therefore no additional information can be gained.[29] We previously demonstrated that cluster mobility can be observed via one-bond proton-silver *J*-couplings in hydrido silver clusters.[30-34] For example, $[Ag_7(H)(S_2CC(CN)_2)_6]^{6-}$ showed an octet of octets resonance in the ^{1}H NMR spectrum at room temperature, which was assigned to the central hydride coupled to the seven magnetically equivalent silver nuclei.[30] These spectroscopic evidences can be tentatively explained by rapid Ag intracluster exchange on the octahedron in solution, for example through a mechanism of triangular rotations.[35] Another possibility is rapid ligand exchange. We note that in **1**, the average Ag-P bond dissociation energy is computed to be 0.86 eV (see DFT calculations below), a value significantly lower than its Ag-S counterpart (1.25 eV). On the other hand, a dtp ligand coordinated to an Ag_3 triangle can move nearly freely on it by exchanging various η^3 and/or η^4 coordination modes (see below). We therefore suggest a ligand exchange process initiated by (partial) dppm decoordination coupled with soft dtp coordination changes. This scenario is also supported by the fact that we could not identify by exploratory DFT calculations any transition state associated with exchange of Ag positions on the octahedron.

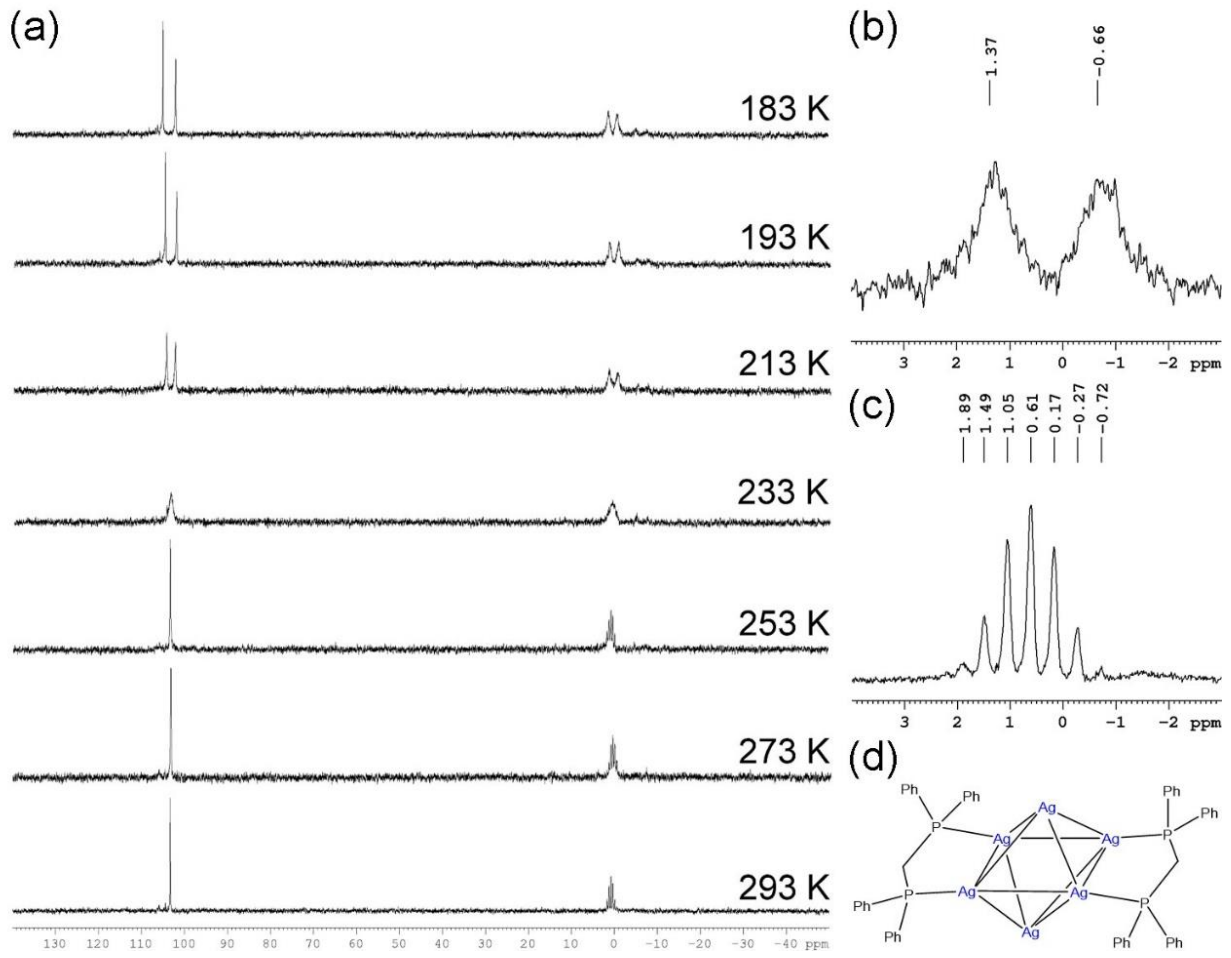

Figure 2. (a) VT $^{31}P\{^{1}H\}$ NMR spectrum of **1** in CD_2Cl_2. (b) P-Ag coupling in the $^{31}P\{^{1}H\}$ NMR spectrum at 183K and (c) 293 K. (d) Schematic presentation of the bridging mode of dppm ligands.

The ESI mass spectrum of **1** shows two molecular ion peaks at *m/z* 2375.1858 and 2413.1868 which correspond to the silver adducts of $[\mathbf{1} + Ag^+]^+$ (calc. *m/z* 2374.6431) and $[\mathbf{1} + Ag^+ + 2(H_2O)]^+$ (calc. *m/z* 2412.6647), respectively (Figure 3). Other fragments such as $[Ag_5(dtp)_2(dppm)_2]^+$ (calc. *m/z* 1732.7987), $[Ag_5(dtp)_1(dppm)_2 - H^+]^+$ (calc. *m/z* 1518.7736), $[Ag_3(dtp)_2(dppm)_1]^+$ (calc. *m/z* 1134.8688), and $[Ag_2(dtp)_1(dppm)_1]^+$ (calc. *m/z* 812.9468) can also be observed. It is noted that silver clusters connected to both dtp and dppm ligands are rarely

reported.[36,37] The fragmentation occurring in the gas phase can be related to the cluster instability in solution. When compound **1** is dissolved in solutions such as chloroform, dichloromethane, or THF, the color gradually changes from yellow to dark purple. It indicates that a further reaction occurs, which can be monitored by time-dependent $^{31}P\{^{1}H\}$ NMR spectroscopy (Figure S7). The resonances of **1** at 103.2 and 0.65 ppm decrease in intensity over time, indicating a gradual decomposition of compound **1**. A two-electron species, $[Ag_{10}\{S_2P(O^iPr)_2\}_8]$,[9] which depicts distinct ^{31}P resonances at 104.3 and 105.8 ppm, is formed upon dissolution within 30 minutes. The formation of unidentified species is observed after 60 minutes at 105.1, 105.7 (broad), and -3.3 ppm (doublet, J_{PAg} = 446 Hz), respectively, accompanied by $dppmO_2$ at 24.7 ppm. The resonance of dppm changes from 0.65 (in **1**) to -3.3 ppm, as well as the splitting pattern from a septet to a doublet. The latter suggests that dppm could be in a bridging mode with each P atom connecting to one Ag atom. The mixture can be separated on a TLC plate using a mixed solvent of Et_2O and hexane (v/v =1:9, Figure S8). The purple band was collected then re-crystallized to obtain crystals of the previously published $[Ag_{10}\{S_2P(O^iPr)_2\}_8]$. Unfortunately, single crystals of another species displaying orange emission under UV light could not be obtained. This result shows that **1** is an intermediate nanocluster proceeding another superatom-to-superatom transformation. In contrast, **1** is much stable in the solid state than in solution.

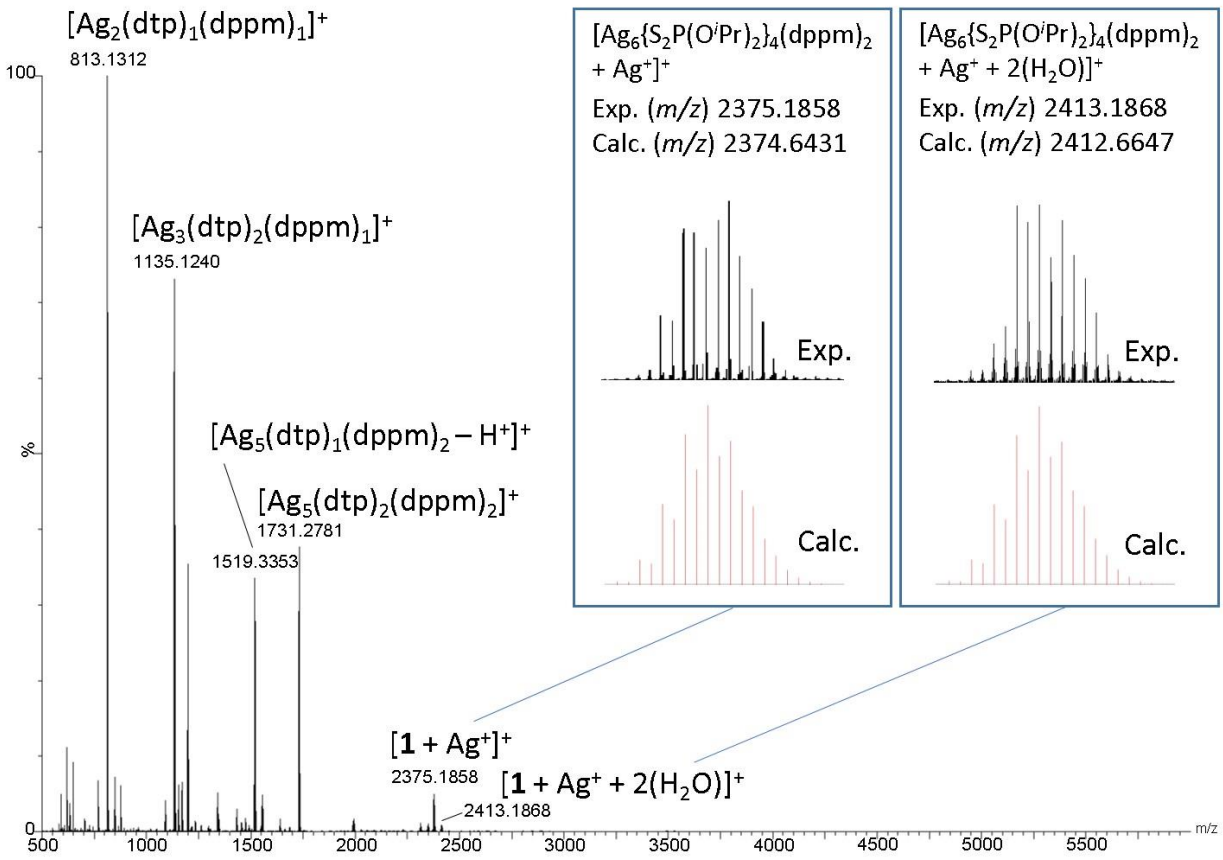

Figure 3. The positive-mode ESI-MS of **1**.

The UV-vis absorption spectrum (Figure 4a) of **1** in CH_2Cl_2 shows two prominent bands at 378 nm (ε = 15,700 M^{-1} cm^{-1}) and 270 nm (ε = 66,300 M^{-1} cm^{-1}). Cluster **1** in solid state emits bright yellow light at ambient temperature with a maximum emission wavelength of 598 nm (Figure 4b) and is slightly red-shifted to 629 nm at 77K. The excitation maximum of **1** around 366 nm (r.t.) matches with its absorption band at 378 nm. A second excitation maximum at 401 nm appears at 77K. Time-resolved photoluminescence (PL) spectra of **1** at 298K (Figure S10) and 77K (Figure S11) exhibit single-exponential decay with lifetimes at nanosecond scale (2.04 ns at 298K; 7.07 ns at 77K), indicating the fluorescence nature of the emission. The PL quantum yield

at 298K is approximately 16.3% (Figure S11), associated with slightly faster non-radiative decay ($k_{nr} = 4.10 \times 10^8$ s^{-1}) than radiative decay ($k_r = 7.99 \times 10^7$ s^{-1}, see Table 2).

It is of note that other two-electron species, $[Ag_6(3S)_4(tfa)_4]$ (tfa = trifluoroacetate),[25] $[Ag_8(pfga)_6]^{2-}$ [38] and $[Ag_{10}\{S_2P(O^iPr)_2\}_8]$,[9] also show strong fluorescence at ambient temperature, with solid-state emission wavelength (r.t.) of 553, 612 and 762 nm, respectively, showing a trend indicating a decrease in their HOMO-LUMO gaps. A solid containing two co-crystallized Ag_6 clusters, namely the 2-electron $[Ag_6(3S)_4(OTf)_4]$ and the 0-electron $[Ag_6(3S)_4(C \equiv C^tBu)_4]^{2+}$ species, exhibits also a yellow emission at 535 nm.[25]

Unlike the red-shift solid state emission spectra observed in **1** upon lowering the temperature, $[Ag_{10}\{S_2P(O^iPr)_2\}_8]$ shows a blue shift from 762 nm (r.t.) to 693 nm (77K, Figure S9).[9] Presumably the thermochromism, which is commonly observed on the emission wavelength difference in the ultrasmall NCs,[39] is very sensitive to their size, nuclearity and shape. The PL properties of **1** in solution are not reported due to its instability in common organic solvents. This is consistent with its ligand fluxional behavior in solution, as demonstrated by time-dependent $^{31}P\{^1H\}$ NMR spectroscopy (*vide supra*).

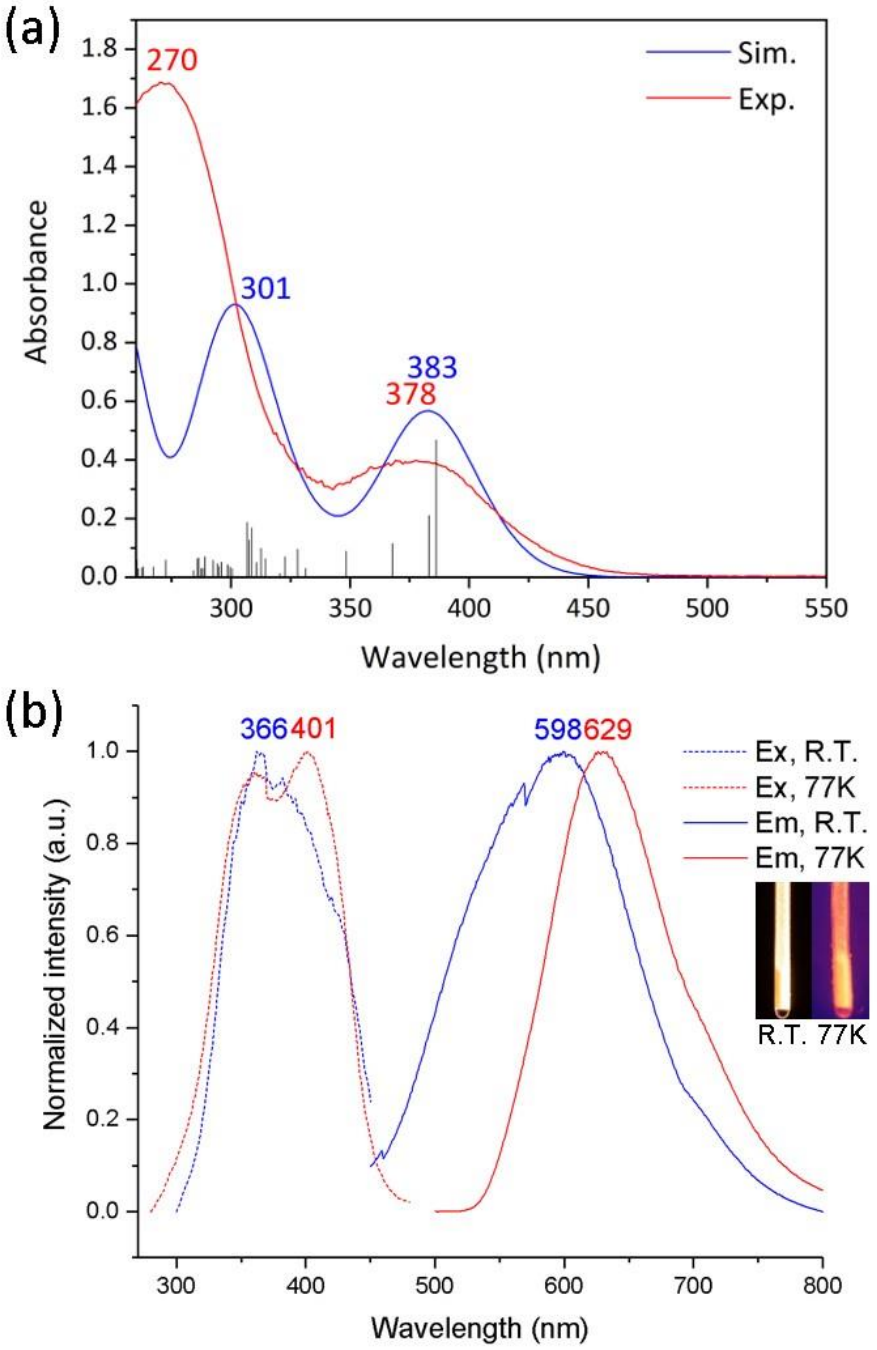

Figure 4. (a) Experimental (red) and simulated (blue) absorption spectra (CH_2Cl_2, r.t.) of **1**. The stick lines (black) refer to the computed individual transitions (the bar heights are proportional to the oscillator strengths). (b) The excitation (dash traces) and emission (solid traces) spectra of **1** in solid at r.t. (blue) and 77K (red).

Table 2. The photophysical data of **1**.

State	Absorbance λ_{abs} (nm), ε (M^{-1} cm^{-1})	Excitation λ_{ex} (nm)	Emission λ_{em} (nm)	Lifetime (ns)	Quantum Yield (%)	k_r (s^{-1})[a]	k_{nr} (s^{-1})[b]
Solid, 298K		366	598	2.04	16.3	7.99×10^7	4.10×10^8
Solid, 77K		401	629	7.07			
Solution, 298K	270 (66,300), 378 (15,700)	Sim.					

[a] k_r: radiative decay. [b] k_{nr}: nonradiative decay. $\tau = \frac{1}{k_r + k_{nr}}$ $QY = \frac{k_r}{k_r + k_{nr}}$

In order to shed some light on the electronic structure of **1**, density functional theory (DFT) calculations at the PBE0/Def2-TZVP level were performed on this compound (see Computational Details). We first addressed the question of molecular configuration by running geometry optimizations with the starting geometries of molecules **I** and **II** taken from the crystal X-ray structure of **1** (*vide supra*). Both optimizations converged to structures of type **I**; *i.e.*, L_A adopting trimetallic tetraconnectivity (η^3: μ_2, μ_2). These two optimized structures, both characterized as true energy minima by vibrational frequency calculations, are almost isoenergetic (ΔE = 0.05 eV; ΔG = 0.04 eV) and exhibit quite similar metrics. Their non-perfect structural identities reflect the (relative) flatness of the potential energy hypersurface around its minimum and is consistent with the molecular ligand fluxionality evidenced by the RT NMR behavior of **1**. It is of note that the simplified model $[Ag_6\{S_2PH_2\}_4(dppm)_2]$ provided similar results, with even less differences between the two optimized structures, as expected from the dtp simplification. Therefore, in the following, we discuss only the results obtained through the optimization of the molecular structure

I. Its major metric data are given in Table 1. There is a good match with the X-ray structure of molecule **I**, with an overestimation by around 2 % of the Ag-Ag contacts, as expected at the level of theory. Its Kohn-Sham orbital diagram (Figure 5) exhibits a substantial HOMO-LUMO gap of 3.85 eV. The HOMO, which lies 0.56 eV above the HOMO-1, can be considered as the 1S superatomic orbital. The LUMO+1, LUMO+2 and LUMO+15 can be identified as the 1P superatomic orbitals, but with significant ligand admixture. Their splitting in energy is in a large part related to the cluster anisotropy induced by its heteroleptic nature. The averaged metal natural atomic orbital (NAO) charges of the Ag atoms is 0.46, a value consistent with the superatomic 2-electron count.[9] The Ag-Ag Wiberg bond indices (avged. 0.1080) are consistent with the existence of some covalent bonding associated with the 1S bonding electron pair.

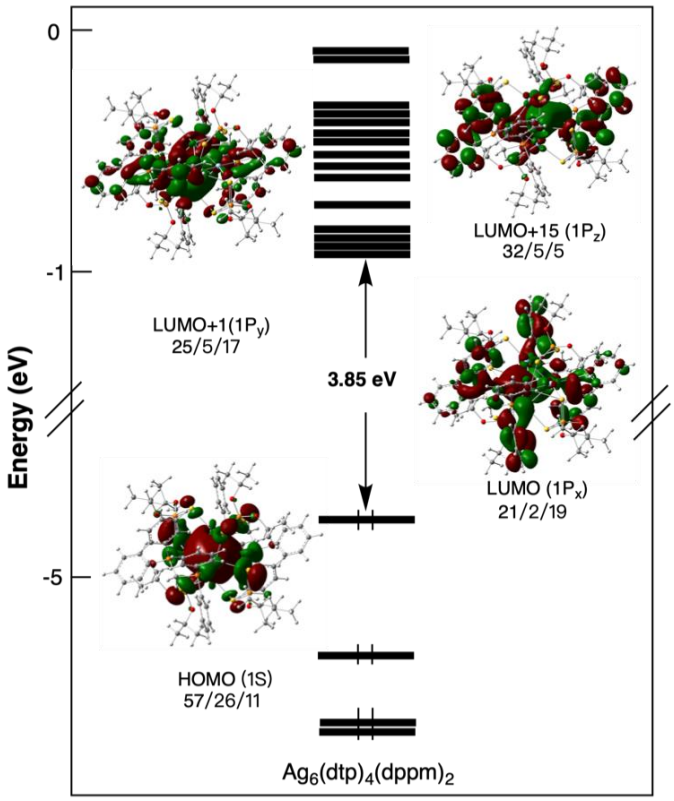

Figure 5. Kohn–Sham orbital diagram of **1**. The MO localizations (in %) are given in the following order: Ag/S/P.

Time-dependent-DFT (TD-DFT) calculations at the same level of theory were also performed to rationalize the optical properties of **1**. The corresponding simulated UV-vis spectrum (see Computational details) is in a quite good agreement with the experimental one (Figure 4a). The low energy band experimentally centered at 378 nm (simulated at 383 nm) is essentially associated with a HOMO(1S)→LUMO($1P_x$) transition. Compared to the 2-electron $[Ag_{10}\{S_2P(O^iPr)_2\}_8]$ relative, whose band of lower energy was computed at 509 nm, with a HOMO-LUMO gap of 3.05 eV (PBE0/Def2-TZVP level), **1** exhibits a substantially larger HOMO-LUMO gap, mainly due to a larger (antibonding) ligand contribution to the LUMO. The next band on the simulated spectrum of **1** originates from a mixture of $4d_{Ag}$→LUMO($1P_x$), HOMO(1S)→ligand and $4d_{Ag}$→ligand transitions. The higher energy transitions computed at around 250 nm are mainly of $4d_{Ag}$→ligand nature.

CONCLUSIONS

In summary, a new methodology to achieve nanocluster-to-nanocluster structural transformation has been designed. The destabilization of the Ag_{20} NC was carried out by adding dppm ligands at 40 °C. Under mild conditions, dppm is competitive with the dtp ligand and acts as a chemical scissor for lowering the NC nuclearity. The metal framework is transformed from an icosahedron-based Ag_{20} to an octahedral Ag_6, accompanied by a change of electron count from eight to two. Temperature-dependent $^{31}P\{^1H\}$ and ^1H NMR spectra of **1** confirm the fast atomic movement at ambient temperature and its slowing down at 183K, the latter spectrum matching well with the solid-state structure. Compound **1** is highly luminescent, the emission being likely of 1P→1S

nature, with a QY of 16.3% in the solid state which prevents fluxionality and minimizes non-radiative vibrational decay. Furthermore, another two-electron species, $[Ag_{10}\{S_2P(O^iPr)_2\}_8]$, can be formed upon dissolving **1** in solution. Therefore, **1** is an intermediate nanocluster of moderate stability in a cluster growth process, in agreement with the differences in the computed ligand-to-cluster bonding averaged energies (dithiophosphate: 4.36 eV; diphosphine: 1.72 eV). This work provides new insight into the ligand-induced structural transformation between nanoclusters.

EXPERIMENTAL SECTION

All chemicals used as received were purchased from commercial sources. Solvents were purified following standard protocols.[40] All reactions were performed in oven-dried Schlenk glassware using standard inert atmosphere techniques. All reactions were carried out under N_2 atmosphere by using standard Schlenk techniques. The ^1H and $^{31}P\{^1H\}$ NMR spectra were recorded on a Bruker Avance II 400 MHz NMR spectrometer, operating at 400.13 MHz for ^1H, and 161.98 MHz for ^{31}P. The chemical shifts (δ) and coupling constants (J) are reported in ppm and Hz, respectively. X-ray diffraction data were collected on a Bruker APEX II CCD diffractometer. UV-visible absorption spectra were measured on a Perkin Elmer Lambda 750 spectrophotometer using quartz cells with path length of 1 cm. The emission, lifetime, and quantum yield spectra were recorded on an Edinburgh FLS920 fluorescence spectrometer.

Synthesis of $[Ag_6\{S_2P(O^iPr)_2\}_4(dppm)_2]$ (1). $[Ag_{20}\{S_2P(O^iPr)_2\}_{12}]$ was prepared by a previously reported method.[12] $[Ag_{20}\{S_2P(O^iPr)_2\}_{12}]$ (0.1343 g, 0.028 mmol) and Bis(diphenylphosphino)methane (0.1423 g, 0.370 mmol) were dissolved in THF (30 mL), kept stirring at 40 °C in dark for 24h. The yellowish brown solution was dried under vacuum. The product was washed with DI-H_2O (10 mL x 3) and then extracted by CH_2Cl_2 (30 mL). The solution was filtered and dried. The product was washed by MeOH, and the precipitate was collected and

dried to yield a yellow powder as $[Ag_6\{S_2P(O^iPr)_2\}_4(dppm)_2]$. Yield: 0.0481 g (22.3%, based on Ag). $^{31}P\{^1H\}$ NMR (161.98 MHz, CD_2Cl_2, δ, ppm, 293K): 103.2 (S_2P), 0.65 (sept, $^1J_{PAg}$ = 72 Hz, dppm). $^{31}P\{^1H\}$ NMR (161.98 MHz, CD_2Cl_2, δ, ppm, 183K): 102.1 (s, S_2P), 105.0 (s, S_2P), 0.36 (d, $^1J_{PAg}$ = 325 Hz, dppm). ^1H NMR (300.13 MHz, $CDCl_3$, δ, ppm, 293K): 0.98 (d, $^3J_{HH}$ = 7 Hz, 48H, CH_3), 2.99 (br, 4H, CH_2), 4.48 (m, 8H, OCH), 7.24 (m, 25H, *meta*- and *para*- protons on phenyl rings), 7.73 (br, 15H, *ortho*- protons on phenyl rings). UV–Vis [λ in nm (ε in M^{-1} cm^{-1})]: 270 (66,300), 378 (15,700).

X-ray Crystallography. Single crystals suitable for X-ray diffraction analysis of **1** were obtained by slow diffusion of *n*-hexane into dichloromethane solution of the compound at 4°C within a week. Single crystals were mounted on the tip of a glass fiber with epoxy resin. Data were collected on a Bruker APEX II CCD diffractometer using graphite monochromated Mo Kα radiation (λ = 0.71073 Å) at 296K. Absorption corrections for area detector were performed with SADABS[41] and the integration of raw data frame was performed with SAINT.[42] The structures were solved by direct methods and refined by least-squares against F^2 using the SHELXL-2018/3 package,[43] incorporated in SHELXTL/PC V6.14.[44] All non-hydrogen atoms were refined anisotropically. CCDC no. 2202272 contains the supplementary crystallographic data for compound **1** in this article. These data can be obtained free of charge from The Cambridge Crystallographic Data Centre via www. ccdc.cam.ac.uk/data_request/cif.

Computational details. DFT calculations were carried out with the use of the Gaussian 16 program.[45] The valence triple-zeta polarization functions (def2-TZVP)[46,47] basis set was used, together with the Perdew-Burke-Ernzerhof (PBE0)[48,49] correlation functional. All the optimized structures were confirmed as true minima on their potential energy surface by analytical vibration

frequency calculations. The compositions of the molecular orbitals were calculated using the AOMix program.[50] Natural atomic orbital (NAO) populations and Wiberg bond indices were computed with the natural bond orbital NBO 6.0 program [51-53] implemented in the Gaussian 16 package. The UV-visible transitions were calculated by means of TD-DFT calculations at the same level of theory. The UV–visible spectrum weas simulated from the computed TD-DFT transitions and their oscillator strengths by using the SWizard program,[54] each transition being associated with a Gaussian function of half-height width equal to 3000 cm^{-1}.

ASSOCIATED CONTENT

Supporting Information.

The Supporting Information is available free of charge at https://pubs.acs.org/doi/10.1021/acs.inorgchem.xxxxxxx.

Multinuclear NMR spectra, photophysical data, and computational results (PDF)

AUTHOR INFORMATION

Corresponding Authors

C. W. Liu − Department of Chemistry, National Dong Hwa University, Hualien 974301, Taiwan (Republic of China); orcid.org/0000-0003-0801-6499; Email: chenwei@gms.ndhu.edu.tw; Homepage: http://faculty.ndhu.edu.tw/~cwl/index.htm

Jean-Yves Saillard − Univ Rennes, CNRS, F-35000 Rennes, France; orcid.org/0000-0003-4469-7922; E-mail: jeanyves.saillard@univ-rennes1.fr

Authors

Yu-Ming Tseng − Department of Chemistry, National Dong Hwa University, Hualien 974301, Taiwan (Republic of China)

Jian-Hong Liao − Department of Chemistry, National Dong Hwa University, Hualien 974301, Taiwan (Republic of China); orcid.org/0000-0002-7947-1790

Tzu-Hao Chiu − Department of Chemistry, National Dong Hwa University, Hualien 974301, Taiwan (Republic of China); orcid.org/0000-0001-8697-8840

Hao Liang − Univ Rennes, CNRS, F-35000 Rennes, France

Samia Kahlal − Univ Rennes, CNRS, F-35000 Rennes, France; orcid.org/0000-0001-5719-553X

Notes

The authors declare no competing financial interest

ACKNOWLEDGMENT

This work was supported by the National Science and Technology Council (111-2123-M-259-002), and the GENCI computing resource (grant A0090807367). The authors gratefully acknowledge the Instrumentation Center of National Taiwan Normal University (NSTC 111-2731-M-003-001). HL thanks the China Scholarship Council for a Ph.D. grant.

REFERENCES

1. Du, X.; Jin, R. Atomically Precise Metal Nanoclusters for Catalysis. *ACS Nano* **2019**, *13*, 7383-7387.

2. Maity, S.; Bain, D.; Patra, A. An overview on the current understanding of the photophysical properties of metal nanoclusters and their potential applications. *Nanoscale* **2019**, *11*, 22685-22723.
3. Tang, J.; Shi, H.; Ma, G.; Luo, L.; Tang, Z. Ultrasmall Au and Ag Nanoclusters for Biomedical Applications: A Review. *Front. Bioeng. Biotechnol.* **2020**, *8*, 1019.
4. Yang, J.; Pang, R.; Song, D.; Li, M.-B. Tailoring silver nanoclusters via doping: advances and opportunities. *Nanoscale Adv.* **2021**, *3*, 2411-2422.
5. Wang, S.; Li, Q.; Kang, X.; Zhu, M. Customizing the Structure, Composition, and Properties of Alloy Nanoclusters by Metal Exchange. *Acc. Chem. Res.* **2018**, *51*, 2784-2792.
6. Sharma, S.; Chakrahari, K. K.; Saillard, J.-Y.; Liu, C. W. Structurally Precise Dichalcogenolate-Protected Copper and Silver Superatomic Nanoclusters and Their Alloys. *Acc. Res. Chem.* **2018**, *51*, 2475-2483.
7. Wang, Y.; Bürgi, T. Ligand exchange reactions on thiolate-protected gold nanoclusters. *Nanoscale Adv.* **2021**, *3*, 2710-2727.
8. Chang, W.-T.; Lee, P.-Y.; Liao, J.-H.; Chakrahari, K. K.; Kahlal, S.; Liu, Y.-C.; Chiang, M.-H.; Saillard, J.-Y.; Liu, C. W. Eight-Electron Silver and Mixed Gold/Silver Nanoclusters Stabilized by Selenium Donor Ligands. *Angew. Chem. Int. Ed.* **2017**, *56*, 10178-10182.
9. Zhong, Y.-J.; Liao, J.-H.; Chiu, T.-H.; Kahlal, S.; Lin, C.-J.; Saillard, J.-Y.; Liu, C. W. A Two-Electron Silver Superatom Isolated from Thermally Induced Internal Redox Reaction of a Silver(I) Hydride. *Angew. Chem. Int. Ed.* **2021**, *60*, 12712-12716.
10. Ren, X.; Fu, J.; Lin, X.; Fu, X.; Yan, J.; Wu, R.; Liu, C.; Huang, J. Cluster-to-cluster transformation among Au_6, Au_8 and Au_{11} nanoclusters. *Dalton Trans.* **2018**, *47*, 7487-7491.

11. Li, Q.; Luo, T.-Y.; Taylor, M. G.; Wang, S.; Zhu, X.; Song, Y.; Mpourmpakis, G.; Rosi, N. L.; Jin, R. Molecular "surgery" on a 23-gold-atom nanoparticle. *Sci. Adv.* **2017**, *3*, e1603193.
12. Dhayal, R. S.; Lin, Y.-R.; Liao, J.-H.; Chen, Y.-J.; Liu, Y.-C.; Chiang, M.-H.; Kahlal, S.; Saillard, J.-Y.; Liu, C. W. $[Ag_{20}\{S_2P(OR)_2\}_{12}]$: A Superatom Complex with a Chiral Metallic Core and High Potential for Isomerism. *Chem. Eur. J.* **2016**, *22*, 9943-9947.
13. Barik, S. K.; Chiu, T.-H.; Liu, Y.-C.; Chiang, M.-H.; Gam, F.; Chantrenne, I.; Kahlal, S.; Saillard, J.-Y.; Liu, C. W. Mono- and hexa-palladium doped silver nanoclusters stabilized by dithiolates. *Nanoscale* **2019**, *11*, 14581-14586.
14. Chiu, T.-H.; Liao, J.-H.; Gam, F.; Chantrenne, I.; Kahlal, S.; Saillard, J.-Y.; Liu, C. W. Homoleptic platinum/silver superatoms protected by dithiolates: Linear assemblies of two and three centered icosahedra isolobal to Ne_2 and I_3^-. *J. Am. Chem. Soc.* **2019**, *141*, 12957-12961.
15. Zhong, Y.-J.; Liao, J.-H.; Chiu, T.-H.; Gam, F.; Kahlal, S.; Saillard, J.-Y.; Liu, C. W. Doping effect on the structure and properties of eight-electron silver nanoclusters. *J. Chem. Phys.* **2021**, *155*, 034304.
16. Yen, W.-J.; Liao, J.-H.; Chiu, T.-H.; Wen, Y.-S.; Liu, C. W. Homoleptic Silver-Rich Trimetallic M20 Nanocluster. *Inorg. Chem.* **2022**, *61*, 6695-6700.
17. Lin, Y.-R.; Kishore, P. V. V. N.; Liao, J.-H.; Kahlal, S.; Liu, Y.-C.; Chiang, M.-H.; Saillard, J.-Y.; Liu, C. W. Synthesis, structural characterization and transformation of an eight-electron superatomic alloy, $[Au@Ag_{19}\{S_2P(OPr)_2\}_{12}]$. *Nanoscale* **2018**, *10*, 6855-6860.
18. Yue, C.; Yan, C.; Feng, R.; Wu, M.; Chen, L.; Jiang, F.; Hong, M. A Polynuclear d^{10}–d^{10} Metal Complex with Unusual Near-Infrared Luminescence and High Thermal Stability. *Inorg. Chem.* **2009**, *48*, 2873-2879.

19. Wei, Q.-H.; Zhang, L.-Y.; Shi, L.-X.; Chen, Z.-N. Octahedral hexanuclear silver(I) and copper(I) ferrocenylacetylide complexes. *Inorg. Chem. Commun.* **2004**, *7*, 286-288.

20. Yang, H.; Lei, J.; Wu, B.; Wang, Y.; Zhou, M.; Xia, A.; Zheng, L.; Zheng, N. Crystal structure of a luminescent thiolated Ag nanocluster with an octahedral Ag_6^{4+} core. *Chem. Commun.* **2013**, *49*, 300-302.

21. Kikukawa, Y.; Kuroda, Y.; Suzuki, K.; Hibino, M.; Yamaguchi, K.; Muzuno, N. A discrete octahedrally shaped $[Ag_6]^{4+}$ cluster encapsulated within silicotungstate ligands. *Chem. Commun.* **2013**, *49*, 376-378.

22. Wang, Z.-Y.; Wang, M.-Q.; Li, Y.-L.; Luo, P.; Jia, T.-T.; Huang, R.-W.; Zang, S.-Q.; Mak, T. C. W. Atomically Precise Site-Specific Tailoring and Directional Assembly of Superatomic Silver Nanoclusters. *J. Am. Chem. Soc.* **2018**, *140*, 1069-1076.

23. Wang, Z.; Su, H.-F.; Kurmoo, M.; Tung, C.-H.; Sun, D.; Zeng, L.-S. Trapping an octahedral Ag_6 kernel in a seven-fold symmetric Ag_{56} nanowheel. *Nat. Commun.* **2018**, *9*, 2094.

24. Deng, G.; Lee, K.; Deng, H.; Bootharaju, M. S.; Zheng, N.; Hyeon, T. Alkynyl-Protected $Ag_{12}Cu_4$ Cluster with Aggregation-Induced Emission Enhancement. *J. Phys. Chem. C* **2022**, DOI: 10.1021/acs.jpcc.2c04782.

25. Cheng, X.; Zhong, R.-R.; Yuan, S.-F.; Guan, Z.-J.; Liu, K.-G. Compact accumulation of superatomic silver nanoclusters with an octahedral Ag_6 core ligated by trithiane. *Nanoscale* **2022**, *14*, 10321-10326.

26. Huang, J.-H.; Wang, Z.-Y.; Zang, S.-Q.; Mak, T. C. W. Spontaneous Resolution of Chiral Multi-Thiolate-Protected Ag_{30} Nanoclusters. *ACS Cent. Sci.* **2020**, *6*, 1971-1976.

27. Zou, X.; Jin, S.; Du, W.; Li, Y.; Wang, S.; Zhu, M. Multi-ligand-directed synthesis of chiral silver nanocluster. *Nanoscale* **2017**, *9*, 16800-16805.

28. Yuan, S.-F.; Li, P.; Tang, Q.; Wan, X.-K.; Nan, Z.-A.; Jiang, D.-e.; Wang, Q.-M. Alkynyl-protected silver nanoclusters featuring an anticuboctahedral kernel. *Nanoscale* **2017**, *9*, 11405-11409.

29. Liao, J.-H.; Latouche, C.; Li, B.; Kahlal, S.; Saillard, J.-Y.; Liu, C. W. A Twelve-Coordinated Iodide in a Cuboctahedral Silver(I) Skeleton. *Inorg. Chem.* **2014**, *53*, 2260-2267.

30. Liao, P.-K.; Liu, K.-G.; Fang, C.-S.; Wu, Y.-Y.; Liu, C. W. $[Ag_7(H)\{S_2CC(CN)_2\}_6]^{6-}$: An Anionic Heptanuclear Silver Hydride Cluster Compound Stabilized by Dithiolate Ligands. *J. Clust. Sci.* **2019**, *30*, 1185-1193.

31. Liao, P.-K.; Liu, K.-G.; Fang, C.-S.; Liu, C. W.; Jr. Flacker, J. P.; Wu, Y.-Y. A Copper(I) Homocubane Collapses to a Tetracapped Tetrahedron Upon Hydride Insertion. *Inorg. Chem.* **2011**, *50*, 8410-8417.

32. Liao, J.-H.; Chang, H.-W.; Li, Y.-J.; Fang, C.-S.; Sarkar, B.; van Zyl, W. E.; Liu, C. W. Anion templating from a silver(i) dithiophosphate 1D polymer forming discrete cationic and neutral octa- and decanuclear silver(i) clusters. *Dalton Trans.* **2014**, *43*, 12380-12389.

33. Liu, C. W.; Chang, H.-W.; Sarkar, B.; Saillard, J.-Y.; Kahlal, S.; Wu, Y.-Y. Stable Silver(I) Hydride Complexes Supported by Diselenophosphate Ligands. *Inorg. Chem.* **2010**, *49*, 468-475.

34. Liu, C. W.; Chang, H.-W.; Fang, C.-S.; Sarkar, B.; Wang, J.-C. Anion-templated syntheses of octanuclear silver clusters from a silver dithiophosphate chain. *Chem. Commun.* **2010**, *46*, 4571-4573.

35. Zheng, K.; Fung, V.; Yuan, X.; Jiang, D.-e.; Xie, J. Real Time Monitoring of the Dynamic Intracluster Diffusion of Single Gold Atoms into Silver Nanoclusters. *J. Am. Chem. Soc.* **2019**, *141*, 18977-18983.

36. Liu, C. W.; Sarkar, B.; Liaw, B.-J.; Lin, Y.-W.; Lobana, T. S.; Wang, J.-C. The influence of alkane spacer of bis(diphenylphosphino)alkanes on the nuclearity of silver(I): Syntheses and structures of P, P'-bridged clusters and coordination polymers involving dithiophosphates. *J. Organomet. Chem.* **2009**, *694*, 2134-2141.
37. Liu, C. W.; Liaw, B.-J.; Liou, L.-S. Syntheses and structures of silver(I) clusters uniquely exhibiting three distinct binding modes, two of which are novel, for a dithiophosphate ligand. *Inorg. Chem. Commun.* **2004**, *7*, 868-870.
38. Liu, K.-G.; Gao, X.-M.; Liu, T.; Hu, M.-L.; Jiang, D.-e. J. All-Carboxylate-Protected Superatomic Silver Nanocluster with an Unprecedented Rhombohedral Ag_8 Core. *J. Am. Chem. Soc.* **2020**, *142*, 16905-16909.
39. Zhou, M.; Jin, R. Optical Properties and Excited-State Dynamics of Atomically Precise Gold Nanoclusters. *Annu. Rev. Phys. Chem.* **2021**, *72*, 121-142.
40. Perrin, D. D.; Armarego, W. L. F. In *Purification of laboratory chemicals*, 3rd Edition, Pergamon Press, Oxford, 1988.
41. SADABS, version 2014-11.0, Bruker Area Detector Absorption Corrections, Bruker AXS, Inc., Madison, WI, 2014.
42. SAINT, V8.30A, Software for the CCD Detector System, Bruker Analytical, Madison, WI, 2012.
43. Sheldrick, G. M. A short history of SHELX. *Acta Cryst. A* **2008**, *64*, 112.
44. SHELXTL, Version 6.14, Bruker AXS, Inc., Madison, Wisconsin, 2003.
45. Gaussian 16, Revision C.01, Frisch, M. J.; Trucks, G. W.; Schlegel, H. B.; Scuseria, G. E.; Robb, M. A.; Cheeseman, J. R.; Scalmani, G.; Barone, V.; Petersson, G. A.; Nakatsuji, H.; Li, X.; Caricato, M.; Marenich, A. V.; Bloino, J.; Janesko, B. G.; Gomperts, R.; Mennucci, B.;

Hratchian, H. P.; Ortiz, J. V.; Izmaylov, A. F.; Sonnenberg, J. L.; Williams-Young, D.; Ding, F.; Lipparini, F.; Egidi, F.; Goings, J.; Peng, B.; Petrone, A.; Henderson, T.; Ranasinghe, D.; Zakrzewski, V. G.; Gao, J.; Rega, N.; Zheng, G.; Liang, W.; Hada, M.; Ehara, M.; Toyota, K.; Fukuda, R.; Hasegawa, J.; Ishida, M.; Nakajima, T.; Honda, Y.; Kitao, O.; Nakai, H.; Vreven, T.; Throssell, K.; Montgomery, J. A., Jr.; Peralta, J. E.; Ogliaro, F.; Bearpark, M. J.; Heyd, J. J.; Brothers, E. N.; Kudin, K. N.; Staroverov, V. N.; Keith, T. A.; Kobayashi, R.; Normand, J.; Raghavachari, K.; Rendell, A. P.; Burant, J. C.; Iyengar, S. S.; Tomasi, J.; Cossi, M.; Millam, J. M.; Klene, M.; Adamo, C.; Cammi, R.; Ochterski, J. W.; Martin, R. L.; Morokuma, K.; Farkas, O.; Foresman, J. B.; Fox, D. J. Gaussian, Inc., Wallingford CT, 2016.

46. Schaefer, A.; Horn, H.; Ahlrichs, R. J. Fully optimized contracted Gaussian basis sets for atoms Li to Kr. *J. Chem. Phys*. **1992**, *97*, 2571-2577.
47. Schaefer, A.; Huber, C.; Ahlrichs, R. J. Fully optimized contracted Gaussian basis sets of triple zeta valence quality for atoms Li to Kr. *J. Chem. Phys*. **1994**, *100*, 5829-5835.
48. Perdew, J. P.; Ernzerhof, M.; Burke, K. Rationale for Mixing Exact Exchange with Density Functional Approximations. *J. Chem. Phys.* **1996**, *105(22)*, 9982–9985.
49. Adamo, C.; Barone, V. Toward Reliable Density Functional Methods without Adjustable Parameters: The PBE0 Model. *J. Chem. Phys*. **1999**, *110 (13)*, 6158–6170.
50. Gorelsky, S. I. AOMix program,http://www.sg-chem.net.
51. Reed, A. E.; Weinhold, F. Natural Bond Orbital Analysis of Near-Hartree-Fock Water Dimer. *J. Chem. Phys*. **1983**, *78*, 4066-73.
52. Carpenter, J. E.; Weinhold, F. Analysis of the Geometry of the Hydroxymethyl Radical by the Different Hybrids for Different Spins Natural Bond Orbital Procedure. *J. Mol. Struct*. THEOCHEM. **1988**, *169*, 41-62.

53. Reed, A. E.; Curtiss, L. A.; Weinhold, F. Intermolecular Interactions from a Natural Bond Orbital, Donor-Acceptor Viewpoint. *Chem. Rev*. **1988**, *88*, 899-926.

54. Gorelsky, S. I. SWizard program, revision 4.5, http://www.sg-chem.net.